Variation in the organisation and subunit composition of the mammalian pyruvate dehydrogenase complex E2/E3BP core assembly

Vijayakrishnan, S. [*, †, ‡], Callow, P. [§, ‖], Nutley, M.A. [¶], McGow, D. [†], Gilbert, D. [#, $], Kropholler, P.[∞], Cooper, A. [¶], Byron, O. [*] and Lindsay, J.G.[†, 1]

[†] Institute of Molecular, Cell and Systems Biology
College of Medical, Veterinary and Life Sciences
University of Glasgow
Glasgow G12 8QQ, UK

[*] School of Life Sciences
College of Medical, Veterinary and Life Sciences
University of Glasgow
Glasgow G12 8QQ, UK

[‡] MRC-University of Glasgow Centre for Virus Research
8 Church Street
Glasgow G11 5JR, UK

[§] Large Scale Structures Group
Institut Laue Langevin
6 rue Jules Horowitz, 38042 Grenoble
Cedex 9, FRANCE

[‖] EPSAM and ISTM Research Institutes
Keele University
Staffordshire, ST5 5BG, UK

[¶] School of Chemistry
College of Science and Engineering
University of Glasgow
Glasgow, G12 8QQ, UK

[#] School of Information Systems
Computing and Mathematics
Brunel University**,** Uxbridge
Middlesex, UB8 3PH, UK

[$] School of Computing Science
College of Science and Engineering
University of Glasgow
Glasgow, G12 8QQ, UK

[∞] School of Mathematics and Statistics
College of Science and Engineering
University of Glasgow
Glasgow, G12 8QQ, UK

[1] Corresponding author
Email: Gordon.Lindsay@glasgow.ac.uk
Tel: +44 (0) 141 330 4720
Fax: +44 (0) 141 330 5481

SHORT (PAGE HEADING) TITLE: New insights into human PDC core organisation

SYNOPSIS

Crucial to glucose homeostasis in man, the human pyruvate dehydrogenase complex (hPDC) is a massive molecular machine comprising multiple copies of three distinct enzymes (E1-E3) and an accessory subunit, E3 binding protein (E3BP). Its icosahedral E2/E3BP 60-meric ‘core’ provides the central structural and mechanistic framework ensuring favourable E1 and E3 positioning and enzyme cooperativity.

Current core models indicate either a 48E2+12E3BP or 40E2+20E3BP subunit composition. Here, we demonstrate clear differences in subunit content and organisation between recombinant hPDC core (rhPDC; 40E2+20E3BP), generated under defined conditions where E3BP is produced in excess, and its native bovine (48E2+12E3BP) counterpart. Our data provide a rational basis for resolving apparent differences between previous models, both obtained using rhE2/E3BP core assemblies where no account was taken of relative E2 and E3BP expression levels.

Mathematical modeling predicts that an 'average' 48E2+12E3BP core arrangement allows maximum flexibility in assembly while providing the appropriate balance of bound E1 and E3 enzymes for optimal catalytic efficiency and regulatory fine-tuning. We also show that the rhE2/E3BP and bovine E2/E3BP cores bind E3s with a 2:1 stoichiometry and propose that hPDC comprises a heterogeneous population of assemblies incorporating a network of E3 (and possibly E1) cross-bridges above the core surface.

Keywords: pyruvate dehydrogenase complex, E2/E3BP core organisation, E3 binding stoichiometry, ITC, SANS, variable substitution model

ABBREVIATIONS FOOTNOTE:
hPDC, human pyruvate dehydrogenase complex; E3BP, E3 binding protein; LD, lipoyl domain; SBD, subunit binding domain; CTD, C-terminal domain; AUC, analytical ultracentrifugation; SAXS, small angle x-ray scattering; SANS, small angle neutron scattering; PDK, pyruvate dehydrogenase kinase; DD, didomain; rhE2/E3BP, recombinant human E2/E3BP core; rhE3, recombinant human E3; bE2/E3BP native bovine heart E2/E3BP core; cryo-EM, cryo electron microscopy; [^{14}C]-NEM, N-ethyl-1-[^{14}C] maleimide; ITC, isothermal calorimetry; GFC, gel filtration chromatography

INTRODUCTION

The human mitochondrial PDC (hPDC) is a large macromolecular machine (Mr, ~9.5x10^6), responsible for the conversion of pyruvate to acetyl CoA and NADH, the key committed step in carbohydrate utilisation in man. It is assembled from multiple copies of four components: pyruvate decarboxylase (E1), dihydrolipoamide acetyltransferase (E2), dihydrolipoamide dehydrogenase (E3) and E3 binding protein (E3BP). Its E2 and E3BP subunits form a 60-meric pentagonal dodecahedral core to which 20-30 $\alpha_2\beta_2$ E1 tetramers and 6-12 E3 homodimers bind tightly but non-covalently. Human E2 and E3BP have similar modular domain organisations comprising outwardly-extended, N-terminal lipoyl domains (LDs, 2 on E2 and 1 on E3BP), a subunit binding domain (SBD) and a large C-terminal domain (CTD) that mediates core assembly. Individual domains are joined by flexible linkers rich in alanine and proline allowing the peripherally-located LDs to act as 'swinging arms' such that their lipoamide cofactors can visit all 3 active sites in turn during the catalytic cycle. PDC deficiencies have been implicated in a broad range of genetic, metabolic, autoimmune and neurodegenerative disorders [1-7].

PDCs from prokaryotes lack E3BP and the crystal structure of the *Bacillus stearothermophilus* (PDB ID 1B5S) E2-CTD core provides clear insights into its subunit organisation, with the basic building blocks, namely E2 trimers, forming the 20 vertices of the dodecahedron [8]. The mammalian E2/E3BP core is also assembled from 20 trimeric units [9]. Interaction of E3BP with E2 occurs co-translationally and is mediated by their respective CTDs.

The structure and subunit composition of E2/E3BP is critical to the efficient functioning of PDC. Initially it was reported that 12 E3BPs were situated on the 12 pentagonal faces of the E2 assembly in mammalian and yeast PDCs – the so-called 'addition' model of core organisation (60E2+12E3BP) [10, 11]. However, in subsequent 48E2+12E3BP and 40E2+20E3BP 'substitution' models, 12 or 20 E3BPs were proposed to replace an equivalent number of E2s within the 60-meric core structure [12, 13]. Recent analytical ultracentrifugation (AUC) studies, small angle x-ray (SAXS) and neutron scattering (SANS) solution structures combined with cryo electron microscopy (cryo-EM) reconstructions of human recombinant E2/E3BP (rhE2/E3BP) assemblies reveal the presence of open pentagonal faces, strongly supporting the substitution model [12-14].

Current substitution models vary in the trimer population forming the 60-meric core assembly. Thus the 48E2+12E3BP version would be assembled from a mixture of eight E2 homotrimers and twelve 2E2:1E3BP heterotrimers while the 40E2+20E3BP core would be formed exclusively from the latter. The number and distribution of E3BPs within the core is a key issue as overall geometry and subunit composition will influence core stability, catalytic efficiency and pyruvate dehydrogenase kinase (PDK)-mediated regulation [14].

The stoichiometry of E1 and E3 interactions with the central core has also proved controversial. In *B. stearothermophilus* PDC, E1 and E3 bind to E2-SBDs with 1:1 stoichiometries in a mutually exclusive fashion [15-17] whereas, in eukaryotes, E1 binds to a specific E2-SBD and E3 binds exclusively to an equivalent E3BP-SBD in normal circumstances. Crystal structures and solution studies of bacterial E1:E2-SBD [18] and E3:E2-SBD [19] sub-complexes show that association of a second E2-SBD to either E1 or E3 is prevented by steric hindrance. The recent crystal structures of recombinant human E3 (rhE3) bound to E3BP-SBD [20, 21] as well as isothermal calorimetry (ITC) studies of rhE2/E3BP:rhE3 and rhE3BP-SBD:rhE3 interactions [13] suggest a 1:1 stoichiometry [20]. In contrast, a SAXS solution structure of rhE3 complexed with an E3BP-didomain (E3BP-DD, LD plus SBD) indicates a 2:1 (E3BP-DD:E3) relationship [22].

Although considerable structural and biochemical information is available for the individual mammalian PDC components, relatively little is known about the arrangement of its icosahedral E2/E3BP core, including its precise subunit composition, overall organisation and stoichiometry of binding to E1 and E3. Here, we use a range of biochemical and biophysical approaches to demonstrate clear differences in the subunit compositions of native bovine and rhE2/E3BP cores and propose a new variable substitution model. Structural and geometric constraints that govern core organisation and assembly have also been explored by mathematical modeling revealing a plausible basis for favoring the 48E2+12E3BP model *in situ*. Moreover, we show that, at maximal occupancy, the number of E3 homodimers tethered to the assembled E2/E3BP 60-mer is equivalent to 50% of the E3BP subunits present, indicative of a 2E3BP:1E3 stoichiometry and suggesting the presence of a novel architectural feature, namely a network of E3 cross-bridges linking pairs of E3BPs above the core surface.

EXPERIMENTAL

Protein expression and purification

rhE3 (in pET14b) and rhE2/E3BP (in pET11/pET28b) were over-expressed in *E. coli* BL21 star (DE3) cells (Invitrogen), grown in LB media supplemented with the appropriate antibiotics. Cells were induced at OD_{600} 0.6-0.8 with 1 mM IPTG for 4 h at 30°C (rhE3) or 16 h at 15°C (rhE2/E3BP). rhE2/E3BP cultures were supplemented with 100 μg/ml lipoic acid. Cells were harvested (10,000 g for 15 min at 4°C) and over-expression assessed by SDS-PAGE. Cell pellets (in 0.1 M NaCl, 0.01 M imidazole, 50 mM potassium phosphate buffer, pH 8.0 supplemented with EDTA-free protease inhibitors (Roche), DNase I (Sigma) and Halt protease inhibitor cocktail (Thermo Scientific)) were lysed by French press treatment and clarified by centrifugation. Proteins were purified by zinc chelate chromatography on a BioCAD 700E Workstation by virtue of their N-terminal His-tags. In the case of the purified rhE2/E3BP assembly only E3BP-contained a His-tag so isolation of intact rhE2/E3BP core required co-integration of E2 and E3BP. Further purification involved either anion exchange on a high-capacity 20HQ column (rhE2/E3BP) for selective DNA removal (Applied Biosystems, USA) and/or gel filtration (rhE3, rhE2/E3BP) on a Sephacryl S-300 column (Amersham, USA). Excess unincorporated, monomeric E3BP was removed from the high M_r E2/E3BP core during the gel filtration step. Purified enzymes in PEBS100 buffer (2 mM EDTA, 0.01% (w/v) NaN_3, 0.1 M NaCl, 50 mM potassium phosphate, pH 7.5) were analysed by SDS-PAGE. An extinction coefficient of

11,300 $M^{-1}cm^{-1}$ at 450 nm was used for FAD and 1,951,320 $M^{-1}cm^{-1}$ at 280 nm for the rhE2/E3BP assembly using ProtParam (http://www.expasy.ch/tools/protparam.html).

Deuterated E3 (dE3) was over-expressed as follows: plasmid encoding rhE3 was transformed into BL21 (DE3) cells and over-expression carried out in Enfors minimal medium (containing 85% D_2O and hydrogenated glycerol as the carbon source) at 30°C to an OD_{600} of 15 using an Enfors fermentation system. dE3 was purified as for hydrogenated rhE3 and purity assessed by SDS-PAGE.

Bovine heart PDC was purified as described previously [23] with slight modifications. PDC was kept at 4°C in 2 mM EDTA, 0.01% NaN_3, 0.5% (v/v) Triton X-100, 50 mM potassium phosphate buffer, pH 7.4. Subsequently, bovine E2/E3BP core (bE2/E3BP) was purified on discontinuous sucrose gradients [24] and its concentration measured by the Biuret method.

Purified enzymes were exchanged into PEBS100 buffer (or PEBS100 with 0.5% (v/v) Triton X-100) and used within 1-2 days.

Sedimentation velocity analytical ultracentrifugation (SV AUC)

For SV analysis of rhE2/E3BP:rhE3 complexes, samples were maintained at 191.5 nM and the rhE3 concentration varied to achieve E3BP:E3 ratios from 4:1 (48E2/12E3BP:3E3) to 1:4 (48E2/12E3BP:48E3). Samples (360 µl) in PEBS100 buffer were loaded into 12 mm double sector centrepieces and centrifuged at 20,000 rpm, 4°C. Sedimentation profiles acquired with Rayleigh interference optics were analysed using *c(s)* analysis in SEDFIT [25]. The partial specific volumes $\bar{\nu}$ of rhE2/E3BP and rhE3, calculated using SEDNTERP [26], were 0.744 and 0.739 ml/g, respectively at 20°C.

Gel filtration chromatography (GFC)

rhE2/E3BP:rhE3 samples were prepared by maintaining rhE2/E3BP at 0.42 mM and varying rhE3 levels to satisfy rhE2/E3BP:rhE3 ratios ranging from 3:1 (48E2/12E3BP:4E3) to 1:3 (48E2/12E3BP:36E3). Samples were analyzed by Sephacryl S-300 gel filtration with uncomplexed rhE2/E3BP and rhE3 included as controls.

Small angle neutron scattering (SANS)

SANS was conducted on beamline D22 of the Institut Laue-Langevin (ILL), Grenoble at detector distances of 4 and 14 m. Transmission and scattering data (buffer and sample) were recorded for 4 min and 15 min, respectively at 4°C in 1 mm quartz cuvettes, covering an overall momentum transfer (*Q)* range of $0.0034 < Q < 0.143$ $Å^{-1}$. The response of the two-dimensional area gas detector was calibrated against water. Raw data were analyzed using the program $GRAS_{ans}P$ written by Charles Dewhurst, ILL (http://www.ill.eu/instruments-support/instruments-groups/groups/lss/grasp/home/). The *p(r)* distance distribution, maximum dimension (D_{max}) and radius of gyration (R_g) were obtained using the programs PRIMUS [27] and GNOM [28, 29].

[^{14}C]-NEM radio-labeling and counting

Purified PDC (40, 60 and 120 µg) and rhE2/E3BP (20 µg and 40 µg) complexed with rE3 (at stoichiometries of 2:1, 10:1, 20:1 and 40:1) suspended in PEBS100 buffer were radio-labeled with 0.65 mM N-ethyl-1-[^{14}C]maleimide (33.2 mCi/mmol, PerkinElmer) and incubated for 30 min at room temperature. All samples were subsequently mixed with NAD^+ (0.5 mM) or NADH (1 mM) followed by incubation for 10 min at room temperature. Reactions were terminated by the addition of 0.05 M DTT after which SDS loading dye was added. Labeled samples were assessed by SDS-PAGE on 8% (w/v) slab gels (17 cm x 15 cm x 2 mm) at 400 V, 65 mA. Gels were stained, destained, the radioactive

bands excised and dissolved overnight in SOLVABLE (PerkinElmer, UK). Gel pieces from blank tracks were used to estimate background radioactivity. Solubilized samples were mixed with EcoScint A (National Diagnostics, UK) and counted (10 min/sample) in a Beckman LS 6500 scintillation counter. Four bovine PDC and four rhE2/E3BP:E3 preparations were separately radio-labeled. Counts for each were determined in triplicate. Data were analyzed statistically as follows [30]:

$$Ratio\ of\ counts\left(\frac{E2}{E3BP}\right)=\frac{C_{E2}}{C_{E3BP}}\left(1+\frac{\sigma^2_{E3BP}}{C^2_{E3BP}}\right)$$

$$Variance\left(\frac{E2}{E3BP}\right)=\frac{C^2_{E2}}{C^2_{E3BP}}\left(\frac{\sigma^2_{E2}}{C^2_{E2}}+\frac{\sigma^2_{E3BP}}{C^2_{E3BP}}\right)$$

where C_{E2}, C_{E3BP} and σ_{E2}, σ_{E3BP} represent the [^{14}C] counts and associated errors determined for radio-labeled rhE2 and rhE3BP respectively.

Fluorography

To eliminate background labeling of accessible cysteines as a possible source of error in the [^{14}C]-NEM radio-labeling study, fluorographic analysis of rhE2/E3BP:rhE3 was undertaken. Samples of radio-labeled rhE2/E3BP (6 μg) complexed with rhE3 at a stoichiometric ratio of 10:1 were run on 8% SDS-PAGE gels, then stained and fixed overnight. Fluorography was performed as described by Chamberlain [31]. Fixed gels were immersed in Amplify (GE Healthcare) and incubated for 30 min prior to drying under vacuum at 80°C for 2 h. Fluorographs were stored at -80°C and developed on x-ray film (Kodak, UK) after 4-7 days.

Mathematical modeling

The algorithm for modeling the 60-meric core organisation was based on its assembly from 20 trimeric units employing two important constraints: only one E3BP was allowed per trimer and E3BP was allowed to interact only with itself. On this basis, core subunit arrangements ranging from 60E2+0E3BP to a maximum of 40E2+20E3BP can be theoretically envisaged. Dodecahedral faces were parameterized by [X,Y,Z] (the number of pentagonal dodecahedral core faces that incorporate 3, 4, or 5 pairs of E2s, respectively). The resulting set of simultaneous linear constraint equations was solved to obtain a list of solutions for the number of 3-, 4- and 5-E2 pair faces at each E2+E3BP subunit stoichiometry. The equations were implemented as a finite domain constraint logic program in Sicstus Prolog (http://www.sics.se/sicstus*)*, using its inbuilt constraint solver to generate the solutions.

Isothermal titration calorimetry (ITC)

Purified proteins were dialyzed at 4°C in PEBS100 buffer (rhE2/E3BP and rhE3) or PEBS100 plus 0.5% (v/v) Triton X-100 (bE2/E3BP and rhE3). ITC measurements were conducted on a MicroCal VP-ITC titration microcalorimeter at 20°C [32]. Analysis and curve fitting to the binding isotherms using MicroCal ORIGIN v7.0 gave values for the association constant (K_a), the molar ratio (n), and the change in enthalpy (ΔH) for protein-protein interactions.

RESULTS

Titration of the rhE2/E3BP core assembly with increasing amounts of rhE3 indicates saturation at a 2:1 stoichiometry

Initial GFC and AUC studies were conducted to assess the number of E3 dimers tethered to the rhE2/E3BP core at maximal occupancy as a means of assessing binding stoichiometry and E3BP content. The GFC profiles of a series of rhE2/E3BP:rhE3 mixtures (based on the 48E2+12E3BP model) covering ratios from 48E2/12E3BP:4E3 (3:1) to 48E2/12E3BP:36E3 (1:3) are shown in Fig. 1A. The K_ds, for rhE3BP:rhE3 and E3BP-DD:E3 sub-complex formation are reported to be 6.3 nM and 35.7 nM, respectively [24, 33]. E3 and E3BP concentrations used here were in the low μM range, ensuring tight and complete binding.

Void volume peaks (38 ml) for the high M_r rhE2/E3BP core uncomplexed and complexed with rhE3 were apparent at all ratios, whereas free rhE3 (V_e 65 ml) was evident only in the range 1:1 to 1:3, i.e. 12-36 E3 dimers per 48E2/12E3BP core. SDS-PAGE analysis confirmed the presence of free E3 at these ratios (Supplementary Fig. S1). These estimates of maximal E3 binding to assembled E2:E3BP core indicated that saturation was achieved prior to addition of 12 E3BPs per core and supported our previous data indicating 2:1 binding between a free (monomeric) truncated version of E3BP (lipoyl domain plus adjacent subunit binding domain) and E3 [22].

Sedimentation velocity AUC analysis was also conducted for a similar series of rhE2/E3BP:rhE3 mixtures and resultant profiles were analysed using the *c(s)* model in SEDFIT [25] (Fig. 1B). $s^0_{20,w}$ for free rhE3 was 5.8 S, in agreement with previous data [22]. An increase in sedimentation coefficient for the rhE2/E3BP core from 29.3 to 35.3 S was observed on rhE3 binding. Moreover, uncomplexed rhE3 became detectable at a 1:1 stoichiometry (12 E3 dimers per 48E2/12E3BP core), again consistent with 2:1 binding. GFC and AUC studies were designed on the basis of the 48E2+12E3BP substitution model; however, the presence of excess rhE3 at 12 E3 dimers per core is also consistent with a 40E2+20E3BP model with rhE3 saturation occurring at 10 E3s for a 2:1 stoichiometry in this case.

Ten rhE3s bind to the rhE2/E3BP core

To establish the binding stoichiometry and assess the rhE2/E3BP core composition more precisely, rhE2/E3BP was reconstituted with increasing amounts of deuterated E3 (dE3) and complex formation monitored by SANS. Given the high molecular weight of the rhE2/E3BP core assembly (~3.5 MDa) compared with E3 (106 kDa), accurate titration measurements of hydrogenated E3 binding using SAXS would prove difficult. By exploiting neutron scattering, it was possible to increase the E3 signal by deuteration, markedly enhancing the sensitivity of stoichiometry measurements. Scattering curves for rhE2/E3BP and rhE2/E3BP:dE3 obtained at various levels of dE3 saturation are shown in Fig. 2A. Intensity increases, particularly in the low angle region, were clearly evident on dE3 addition, over a stoichiometry range from 0 (uncomplexed rhE2/E3BP) to 18 dE3 dimers per core. As expected, dE3 attachment to rhE2/E3BP results in an increased radius of gyration, R_g and scattering intensity at zero angle, *I(0)* (Table 1). Moreover, dE3 addition yielded a maximum R_g of 162 Å for the E2/E3BP:E3 sub-complex, in agreement with a previous report [12]. The *I(0)* value, normalized for concentration, and plotted against the number of dE3s present per core is shown in Fig. 2B. Importantly, at 10 dE3 dimers bound per core, the gradient of the line changes markedly, indicating saturation.

The observed saturation value is close to the published value of 12:1 [12] and could be interpreted as evidence for 1:1 binding assuming the 48E2+12E3BP substitution model. On repeated measurement, however, saturation was always obtained at exactly 10 dE3 dimers per rhE2/E3BP core. Furthermore, possible dE3 aggregation was eliminated as a source of error. Additionally, the R_g (34 Å) and D_{max} (130 Å) values for dE3 (Supplementary Fig. S2) compare well with published data for hydrogenated E3 (38 Å and 130 Å), indicating no major structural changes on E3 deuteration [22]. A marked increase in

particle diameter, D_{max}, from 462 Å to 520 Å was also evident from the rhE2/E3BP *p(r)* distribution function on dE3 saturation (Supplementary Fig. S3).

Since E3 interactions with the intact E2/E3BP scaffold will be governed by core geometry, such stoichiometry measurements are more physiologically relevant than previous analyses of E3 binding to monomeric E3BP-SBD or DD constructs [13, 19-22]. However, a 1:1 stoichiometry is observed in crystal structures of E3-DD and SBD sub-complexes [19-21] where steric hindrance prevents access to a putative second binding site located near the twofold axis of symmetry. It is possible that crystal packing could account for this key difference implying that the E3 crystal structure differs significantly from its structure in solution. In this regard, the D_{max} for protonated or deuterated E3 (determined by SAXS and SANS) is 130Å [22], (Fig. S2) compared with 100Å in the crystal structure indicating that E3 adopts a more open and dynamic conformation in solution. Thus, a plausible explanation for the SANS-based estimate of 10 E3 binding sites per core is that it represents 2:1 binding to a 40E2+20E3BP assembly.

Distinctive subunit organisation of the rhE2/E3BP and bE2/E3BP cores

As already indicated, there are currently two conflicting 48E2+12E3BP and 40E2+20E3BP substitution models for rhPDC core subunit content and organisation in which 12 or 20 E3BPs are proposed to replace an equivalent number of E2s within the 60-meric assembly [12, 13]. Importantly, evidence for both these models was obtained with rhE2/E3BP cores produced using similar recombinant vectors, overexpression systems and protein purification regimes. However, no data were provided on the relative levels of E2 and E3BP expression in either case. Our present study relies on the presence of a His-tag on E3BP for the isolation of the integrated rhE2/E3BP core. Excess monomeric E3BP is always present after the initial purification step prior to its removal by gel filtration ensuring maximal E3BP incorporation. Interestingly, however, previous studies on native bovine heart and yeast PDCs all report the presence of only 12 E3BP subunits per core (i.e. 48E2+12E3BP) [10,11]. Importantly, both models yield predictable and distinct numbers of bound E3s at saturation (Supplementary Table S1).

In view of these conflicting reports, NADH-induced E2 and E3BP lipoamide group radio-labeling was performed to assess possible differences between native bovine (bE2/E3BP) and human (rhE2/E3BP) cores. Specific [^{14}C]-NEM modification of reduced E2 and E3BP lipoamide thiols is achieved in the presence of NADH and catalytic amounts of rhE3. The ratio of [^{14}C]-NEM incorporated into E2 (2LDs) and E3BP (1LD) subunits alters significantly depending on the model in question (Table 2). In particular, a marked difference in ratios is predicted for the 48E2+12E3BP (8:1) [12] and 40E2+20E3BP substitution models (4:1) [13], while potential variations in ratio for E2+E3BP core compositions in the range 44E2+16E3BP (5.5:1) to 40E2+20E3BP (4:1) are relatively minor (Table 2). Radio-labeling was conducted for triplicate samples of four bovine heart PDC and human rhE2/E3BP:rhE3 preparations, to prevent uncertainties owing to batch variation or sample degradation.

Ratio analysis of radio-labeled subunits in rhE2/E3BP and native bE2/E3BP cores is shown in Table 3. Values for the bE2/E3BP core supported the 48E2+12E3BP model (8:1, Table 2), as reported previously [12], while rhE2/E3BP cores generally gave values (4:1) consistent with the 40E2+20E3BP model [13]. Occasional higher values were obtained in the latter case with 5.63, the highest ratio observed, equivalent to a 44E2+16E3BP composition. In summary, radio-labeling data suggested distinctive core models with average compositions of 48E2+12E3BP for bE2/E3BP and approaching 40E2+20E3BP for rhE2/E3BP.

To eliminate background labeling of accessible cysteines as a possible source of error, fluorographic analysis of rhE2/E3BP:rhE3 (Supplementary Fig. S4) was conducted after modification with [^{14}C]-NEM in the presence of NAD^+ or NADH to maintain the E2 and E3BP-linked lipoamide moieties in their oxidised or reduced states. Specific NADH-induced modification of E2 and E3BP was observed with no discernable labeling of complexed rhE3. However, radio-labeling of accessible E3 cysteines, possibly the active-site disulphide pair, was detectable with non-complexed E3 (Supplementary Fig. S4).

Previous studies have established specific modification of E2 and E3BP reduced lipoamide moieties in bovine PDC [34]. Under these conditions, estimates of the rhE2/E3BP core composition obtained by specific NADH-induced [^{14}C] NEM-labeling of E2 and E3BP lipoamide thiols are in agreement with the 40E2+20E3BP model. Brautigam and co-workers [13] provided several lines of evidence for a 40E2:20E3BP core stoichiometry using quantitative Coomassie Blue staining, AUC, native gel electrophoresis and ITC measurements. They also concluded that previous AUC analyses of maximal E1 and E3 binding to the high M_r E2/E3BP core leading to the development of the original 48E2+12 E3BP model by Hiromasa *et al.* [12] were technically flawed. However, neither group took account of the relative levels of E2 and E3BP expression in their systems. This is likely to prove a key factor in determining the final core composition, particularly as E2 itself is capable of self-assembly into a 60-meric icosahedron whereas E3BP is largely monomeric (see Fig. 4) and requires to be co-expressed with E2 to achieve core integration. In this context, it is apparent that generation of recombinant cores with varying E2/E3BP subunit content is a reflection of the relative E2 and E3BP expression levels.

A clear difference in subunit organisation and composition between recombinant human and native bovine cores was also confirmed by ITC. Binding isotherms were generated by titrating rhE3 into the reaction cell containing rhE2/E3BP (Fig. 3A) or bE2/E3BP (Fig. 3B). On curve fitting, molar ratios (*n*, E3BP:E3) of 9.68 ± 0.18 and 5.70 ± 0.09 were obtained for rhE2/E3BP:rhE3 and bE2/E3BP:rhE3, respectively. The E3 titration profile for rhE2/E3BP and bE2/E3BP yielded K_d values with an upper limit of 7 nM and 10 ± 5 nM, respectively, consistent with previously reported values [24, 33] although binding was too tight for accurate measurement. Three independent binding isotherms for rhE2/E3BP:rhE3 and bE2/E3BP:rhE3 complex formation yielded *n* values within 10% of 9.68 and 5.70, respectively, consistent with 2:1 E3BP:E3 binding molar ratios predicted (Supplementary Table S1) for the recombinant 40E2+20E3BP and bovine 48E2+12E3BP models respectively. The recombinant E3:E2/E3BP complex molar ratio (9.68) was also consistent with our SANS data (10 E3 dimers per core),

A problematic issue is that our present ITC and previous biochemical and biophysical analyses [22], all indicating a 2:1 stoichiometry of E3 binding to E3BP using either truncated E3BP constructs or the fully-assembled E2/E3BP core, are in direct contrast to the findings of Brautigam and co-workers [13]. In our case, ITC evaluation of E3 binding to rhE2/E3BP shows saturation at n=10 E3 dimers per core with a maximal K_d of 7 nM. In contrast, Brautigam *et al*. [13] report a much higher K_d (102 nM) that may account for their contrasting n value of 18.8 implying 1:1 E3 binding to a 40E2+20E3BP assembly. In this context, it is noteworthy that PDC-deficient patients totally lacking E3BP retain partial PDC activity (10-20% of controls) suggesting that E3 may still interact with the E2 core to a limited extent in the absence of its normal binding component. In support of this idea, bovine PDC reconstituted *in vitro* with a homogeneous 60-meric E2 core is virtually inactive at stoichiometric E3 levels whereas overall complex activity (approaching 40-50% of wild type) can be restored with a 200-fold E3 excess suggesting that E3 can interact weakly with the normal E1 binding site on E2 under these conditions [35]. Recent surface plasmon resonance data from our laboratory [36] confirm that E3 has a low affinity interaction with a secondary binding site on E2 (K_d ~410 nM) that can lead to partial

E1 displacement at markedly elevated E3 concentrations. This K_d value is only 4-fold higher than the K_d of 102 nM for E3:E3BP complex formation [13] and may account for the additional E3 binding required to achieve saturation in their experiments leading to an erroneously high estimate of E3 binding stoichiometry. In our case, E3 interacts with its primary E3BP binding site with a much lower K_d (7 nM or less) i.e. with at least a 60-fold greater affinity than its weak secondary interaction with E2. It is difficult to assess the reasons underlying these marked differences in E3 binding affinity to the rhE2/E3BP core without a detailed knowledge of the sequences of the E2, E3BP and E3 constructs and recombinant expression system employed by Brautigam and co-workers [13]. Inaccurate protein measurement is another possible source of error in these experiments. In our case, the concentration of purified E2/E3BP and E3 samples was estimated by two independent methods. For E2/E3BP, this involved A_{280} measurement based on the calculated extinction coefficient of the core assembly and Biuret analysis. Possible DNA contamination of purified rhE2/E3BP was eliminated by use of an ion exchange step. E3 concentration was also estimated by the Biuret method and by A_{450} measurement of FAD content after ensuring that protein contained a full complement of cofactor.

E2/E3BP core composition: investigation by mathematical modeling

Mathematical modeling of possible E2/E3BP core arrangements was conducted by systematic variation of E2 homotrimer and 2E2:1E3BP heterotrimer populations that form the 60-meric icosahedron (Supplementary Table S2). Two fundamental constraints were applied to the modeling process: firstly, only one E3BP was allowed per heterotrimer and secondly, E3BPs of neighboring heterotrimers could interact only with each other. The first constraint recognises that E3BP is itself incapable of core formation with no evidence for the existence of 1E2:2E3BP heterotrimers. Thus, despite high rhE3BP expression relative to E2, purified rhE2/E3BP always contains E2 as the major species, as judged by SDS-PAGE and radio-labeling (Supplementary Figs S1 and S4). Justification for the second constraint is that E3BP lacks key residues involved in the hydrophobic 'ball and socket' connection that mediates inter-trimer contacts within the core [12]. It has been suggested that E3BP could self-associate on the core surface [12], and in our earlier AUC studies [14] purified rhE3BP showed little or no capacity to form higher oligomeric states. As shown in Fig. 4, non-specific cross-linking of purified rhE3BP with glutaraldehyde revealed a weak tendency to dimer formation although the majority of rhE3BP remained monomeric. Successful cross-linking of rhE3, a naturally-occurring homodimer, served as a positive control.

Several solutions of core organisation for each model were obtained by mathematical modeling (Table 4). Each represents an E2 and E3BP arrangement that satisfies a particular core composition ranging from 60E2+0E3BP to 40E2+20E3BP. Final states were parameterised by [X,Y,Z] (the number of pentagonal dodecahedral core faces that incorporate 3, 4, or 5 pairs of E2s, respectively). The number of possible final states follows a near Gaussian distribution (Fig. 5A). Importantly, while the 40E2+20E3BP model has only 2 final states (1 symmetric and 1 asymmetric, Fig. 5B), the number of possible states peaks at 7 for the 48E2+12E3BP core (Fig. 5C), with each state showing a distinctive distribution of E3BPs around the core surface. Thus, a 48E2+12E3BP subunit stoichiometry may be advantageous in that it ensures the greatest number of routes to, and final arrangements of, the core structure, enabling rapid and efficient production *in vivo*. Moreover, the relative abundance and distribution of E2 and E3BP subunits will have a direct impact on the number and location of associated E1 and E3 enzymes. Thus, from a functional and regulatory standpoint, a 48E2+12E3BP core composition may be favoured in that it recruits the optimal balance of cognate E1s and E3s for achieving optimal catalytic efficiency and regulatory fine-tuning. E1 normally catalyses the rate-limiting step in the reaction sequence so alterations in bound E1 levels will directly affect the overall

catalytic rate in most circumstances. Interestingly, a reconstituted bovine E2/E3BP core containing only 35% of the normal E3BP complement supports a correspondingly reduced level of PDC activity indicating that the ratio of bound E1s and E3s (as determined by the E2/E3BP core composition) is also important in regulating the overall rate of catalysis [35].

DISCUSSION

Variable subunit composition of the rhE2/E3BP core assembly

Based on current evidence, it is apparent that there is considerable potential for variation in both overall E2/E3BP core organization and subunit stoichiometry. In our case, rhE2 and E3BP co-expression is carried out under conditions where E3BP is produced in excess leading to formation of a 40E2+20E3BP core in support of the hypothesis that only 1E3BP subunit can be incorporated per trimer. We also demonstrate for the first time that, in contrast to E2, rhE3BP was incapable of independent self-assembly into a high M_r 60-meric complex. Indeed, it is largely monomeric with a weak tendency to dimer formation (Fig 4). In this context, we have previously reported that the stability of the rhE2/E3BP core was reduced in comparison with a homogeneous 60-meric E2 core indicating that the E3BP content was likely to influence core 'breathing' and protein dynamics [14, 37].

Advantages in maintaining a standard 48E2+12E3BP core structure in native eukaryotic PDCs

While current evidence lends support to the 40E2+20E3BP model for the rhE2/E3BP core when E3BP is present in excess, we also show that the native bovine assembly has a distinctive 48E2+12E3BP subunit stoichiometry. Interestingly, *in vivo*, E3BP subunit levels per core have always been estimated at 12 in mammalian and yeast PDCs [10, 11] so it will be essential in future to determine whether the 48E2+12E3BP core represents the standard archetypal assembly that has been widely adopted in eukaryotes or if there are characteristic tissue- or species-specific alterations.

As a central 48E2+12E3BP core is composed of two types of trimeric units, namely E2 homotrimers and 2E2/1E3BP heterotrimers, E2 and E3BP synthesis must be tightly coordinated *in vivo* with E3BP being produced in limiting amounts leading to formation of non-uniform cores averaging 12E3BPs per icosahedron. EM studies of PDC have highlighted its inherent heterogeneity [37, 38, 39], so it is also probable that a mixed population of E2/E3BP assemblies is generated *in vivo* such that the 48E2+12E3BP model represents an 'average' structure. As illustrated in Fig. 5, even assuming all cores have a uniform 48E2+12E3BP subunit composition, they can still be arranged in 7 possible final states differing in the distribution of E2 and E3BP subunits around the core surface and consequently the spatial organisation of its interacting E1 and E3 partners.

In summary, on the basis of limited stoichiometry data available to date, the 48E2+12E3BP model appears to represent the standard archetypal PDC core assembly found in eukaryotes although there is undoubtedly potential for significant variation in the subunit content of this central structural framework. Mathematical modeling and biochemical data on E3BP deficient core assemblies also give important insights into potential advantages of deploying a 48E2+12E3BP core composition. In future, it will be essential to determine if there are species or tissue-specific variations in the native E2/E3BP subunit content which has the potential for modulating overall PDC composition leading to subtle alterations in catalytic efficiency and regulatory fine-tuning.

Stoichiometry of E3 interaction with the recombinant human and native bovine E2/E3BP assemblies

Our current results using gel filtration, AUC, SANS and ITC confirm that 10 and 6E3s respectively, bind to individual recombinant human and native bovine E2/E3BP cores respectively at maximal occupancy. These data highlight their distinctive 40E2+20E3BP and 48E2+12E3BP compositions while confirming the 2:1 stoichiometry of E3BP:E3 binding to the surface of these large pentagonal dodecahedral assemblies. It should be noted, however, that final rhPDC core composition is governed by the relative levels of E2 and E3BP expression. Thus the production of a 40E2+20E3BP assembly in recombinant human systems merely reflects one possible scenario, namely where there is excess production of the E3BP subunit (which is never detected *in situ* as an independent, non-integrated species) thereby ensuring its maximal incorporation into the assembling E2 core.

A schematic illustration of an archetypal 48E2+12E3BP core assembly is shown in Fig. 6 with representative E2 and E3BP N-terminal segments, consisting of LDs and SBDs joined by flexible linkers, extending outwards from the core. E3BP content and distribution may vary considerably so the core would be more accurately depicted as a heterogeneous population of closely-related assemblies with an average 48E2+12E3BP composition. Representative E3 cross-bridges linking adjacent pairs of E3BPs are also illustrated. There is an additional possibility of E1 hetero-tetramers linking neighbouring E2-SBDs highlighting the existence of a network of cross-bridges on the core surface (Fig. 6, Movie S1). This architectural feature (a) has the potential to moderate the flexibility of the E2 and E3BP lipoyl 'swinging arms' and (b) may facilitate pyruvate dehydrogenase kinase (PDK) movements around the core. Interestingly, cryo-EM images of rhE2/E3BP reveal the appearance of prominent E3-induced 'spikes' located just above the surface of the CTD. The increased order in this region permits it to be properly resolved on cryo-EM reconstruction, and is consistent with E3 cross-bridge formation restricting movement of the flexible lipoyl 'swinging arms' in this region [14].

AUTHOR CONTRIBUTIONS

SV designed and performed the experiments, analysed the data and wrote the manuscript. PC carried out the SANS experiment and analysis. MAN performed the ITC experiment and analysis. DMcG provided technical support. Mathematical modeling and data analysis was carried out by DG and PK. AC provided conceptual advice on the ITC. OB and JGL supervised the project, designed the experiments and edited the manuscript.

ACKNOWLEDGEMENTS

The authors acknowledge the staff of the ILL-EMBL Deuteration Laboratory for their assistance during sample preparation, the ILL for use of the D22 diffractometer and the EPSRC. We thank Michael Haertlein, Peter Timmins and Trevor Forsyth for advice, support and encouragement. The authors declare that they have no conflict of interest.

FUNDING

This work was partly supported by EPSRC (under grants GR/R99393/01 and EP/C015452/1). SV was the recipient of a Wellcome Trust funded PhD studentship and a Wellcome Trust VIP award. JGL acknowledges continued financial support from BBSRC, UK and the United Mitochondrial Disease

Foundation (UMDF), USA. This research has also benefited from the activities of the DLAB consortium funded by the EU under contracts HPRI–2001–50065 and RII3–CT–2003–505925.

FOOTNOTE

This work was first presented at the 16th European/UK Analytical Ultracentrifuge Meeting 'AUC and Hydro' held at the University of Newcastle, UK in September 2008.

Supplementary information is available at The Biochemical Journal Online.

REFERENCES

1 Blass, J. P. and Gibson, G. E. (1991) The role of oxidative abnormalities in the pathophysiology of Alzheimer's disease. Rev Neurol (Paris). **147**, 513-525

2 Hoyer, S. (2004) Causes and consequences of disturbances of cerebral glucose metabolism in sporadic Alzheimer disease: therapeutic implications. Adv Exp Med Biol. **541**, 135-152

3 Huang, B., Wu, P., Bowker-Kinley, M. M. and Harris, R. A. (2002) Regulation of pyruvate dehydrogenase kinase expression by peroxisome proliferator-activated receptor-alpha ligands, glucocorticoids, and insulin. Diabetes. **51**, 276-283

4 Jones, D. E. (1996) T-cell autoimmunity in primary biliary cirrhosis. Clin Sci (Lond). **91**, 551-558

5 Leung, P. S., Van de Water, J., Coppel, R. L., Nakanuma, Y., Munoz, S. and Gershwin, M. E. (1996) Molecular aspects and the pathological basis of primary biliary cirrhosis. J Autoimmun. **9**, 119-128

6 Mayers, R. M., Leighton, B. and Kilgour, E. (2005) PDH kinase inhibitors: a novel therapy for Type II diabetes? Biochem Soc Trans. **33**, 367-370

7 Robinson, B. H. (1995) Lactic acidemia - disorders of pyruvate carboxylase, pyruvate dehydrogenase. In The Metabolic and Molecular Basis of Inherited Disease (Scriver, C. R., Beaudet, A. L., Sly, W. S. and Valle, D., eds.), pp. 1479-1499, McGraw Hill, New York

8 Izard, T., Aevarsson, A., Allen, M. D., Westphal, A. H., Perham, R. N., de Kok, A. and Hol, W. G. (1999) Principles of quasi-equivalence and Euclidean geometry govern the assembly of cubic and dodecahedral cores of pyruvate dehydrogenase complexes. Proc Natl Acad Sci U S A. **96**, 1240-1245

9 Yu, X., Hiromasa, Y., Tsen, H., Stoops, J. K., Roche, T. E. and Zhou, Z. H. (2008) Structures of the human pyruvate dehydrogenase complex cores: a highly conserved catalytic center with flexible N-terminal domains. Structure. **16**, 104-114

10 Sanderson, S.J., Miller, C. and Lindsay, J.G. (1996) Stoichiometry, organisation and catalytic function of protein X of the pyruvate dehydrogenase complex from bovine heart. Eur J Biochem. **236**, 68-77.

11 Zhou, Z. H., McCarthy, D. B., O'Connor, C. M., Reed, L. J. and Stoops, J. K. (2001) The remarkable structural and functional organization of the eukaryotic pyruvate dehydrogenase complexes. Proc Natl Acad Sci U S A. **98**, 14802-14807

12 Hiromasa, Y., Fujisawa, T., Aso, Y. and Roche, T. E. (2004) Organization of the cores of the mammalian pyruvate dehydrogenase complex formed by E2 and E2 plus the E3-binding protein and their capacities to bind the E1 and E3 components. J Biol Chem. **279**, 6921-6933

13 Brautigam, C. A., Wynn, R. M., Chuang, J. L. and Chuang, D. T. (2009) Subunit and catalytic component stoichiometries of an *in vitro* reconstituted human pyruvate dehydrogenase complex. J Biol Chem. **284**, 13086-13098

14 Vijayakrishnan, S., Kelly, S. M., Callow, P., Bhella, D., Forsyth, T., Lindsay, J.G. and Byron, O. (2010) Solution structure and characterisation of the human pyruvate dehydrogenase complex core assembly. J Mol Biol. **399**, 71-93

15 Hipps, D. S., Packman, L. C., Allen, M. D., Fuller, C., Sakaguchi, K., Appella, E. and Perham, R. N. (1994) The peripheral subunit-binding domain of the dihydrolipoyl acetyltransferase component of the pyruvate dehydrogenase complex of *Bacillus stearothermophilus*: preparation and characterization of its binding to the dihydrolipoyl dehydrogenase component. Biochem J. **297**, 137-143

16 Jung, H. I., Bowden, S. J., Cooper, A. and Perham, R. N. (2002) Thermodynamic analysis of the binding of component enzymes in the assembly of the pyruvate dehydrogenase multienzyme complex of *Bacillus stearothermophilus*. Protein Sci. **11**, 1091-1100

17 Lessard, I. A., Domingo, G. J., Borges, A. and Perham, R. N. (1998) Expression of genes encoding the E2 and E3 components of the *Bacillus stearothermophilus* pyruvate dehydrogenase complex and the stoichiometry of subunit interaction in assembly *in vitro*. Eur J Biochem. **258**, 491-501

18 Frank, R. A., Pratap, J. V., Pei, X. Y., Perham, R. N. and Luisi, B. F. (2005) The molecular origins of specificity in the assembly of a multienzyme complex. Structure. **13**, 1119-1130

19 Mande, S. S., Sarfaty, S., Allen, M. D., Perham, R. N. and Hol, W. G. (1996) Protein-protein interactions in the pyruvate dehydrogenase multienzyme complex: dihydrolipoamide dehydrogenase complexed with the binding domain of dihydrolipoamide acetyltransferase. Structure. **4**, 277-286

20 Ciszak, E. M., Makal, A., Hong, Y. S., Vettaikkorumakankauv, A. K., Korotchkina, L. G. and Patel, M. S. (2006) How dihydrolipoamide dehydrogenase-binding protein binds dihydrolipoamide dehydrogenase in the human pyruvate dehydrogenase complex. J Biol Chem. **281**, 648-655

21 Brautigam, C. A., Wynn, R. M., Chuang, J. L., Machius, M., Tomchick, D. R. and Chuang, D. T. (2006) Structural insight into interactions between dihydrolipoamide dehydrogenase (E3) and E3 binding protein of human pyruvate dehydrogenase complex. Structure. **14**, 611-621

22 Smolle, M., Prior, A. E., Brown, A. E., Cooper, A., Byron, O. and Lindsay, J. G. (2006) A new level of architectural complexity in the human pyruvate dehydrogenase complex. J Biol Chem. **281**, 19772-19780

23 Stanley, C. J. and Perham, R. N. (1980) Purification of 2-oxo acid dehydrogenase multienzyme complexes from ox heart by a new method. Biochem J. **191**, 147-154

24 Smolle, M. (2005) Protein-protein interactions within the human pyruvate dehydrogenase complex. PhD thesis, University of Glasgow, Glasgow

25 Schuck, P. (2000) Size-distribution analysis of macromolecules by sedimentation velocity ultracentrifugation and Lamm equation modeling. Biophys J. **78**, 1606-1619

26 Laue, T. M., Shah, B. D., Ridgeway, T. M. and Pelletier, S. L. (1992) Computer-aided interpretation of analytical sedimentation data for proteins. In Analytical Ultracentrifugation in Biochemistry and Polymer Science (Harding, S. E., Rowe, A. J. and Horton, J. C., eds.), pp. 90-125, Royal Society for Chemistry, London

27 Konarev, P. V., Volkov, V. V., Sokolova, A. V., Koch, M. H. J. and Svergun, D. I. (2003) PRIMUS: a Windows PC-based system for small-angle scattering data analysis. J Appl Cryst. **36**, 1277-1282

28 Semenyuk, A. V. and Svergun, D. I. (1991) GNOM - a program package for small angle scattering data processing. J Appl Cryst. **24**, 537-540

29 Svergun, D. I. (1992) Determination of the regularization parameter in indirect transform methods using perceptual criteria. J Appl Cryst. **25**, 495-503

30 Lynch, M. and Walsh, B. (1997) Genetics and Analysis of Quantitative Traits. Sinauer Association, USA

31 Chamberlain, J. P. (1979) Fluorographic detection of radioactivity in polyacrylamide gels with the water-soluble fluor, sodium salicylate. Anal Biochem. **98**, 132-135

32 Cooper, A. and Johnston, C. M. (1994) In Methods in Molecular Biology, Microscopy, Optical Spectroscopy and Macroscopic Techniques (Jones, C. and Mulloy, B., eds.), pp. 137-150, Humana Press, Totowa, NJ

33 Brown, A. E. (2002) Towards a recombinant model of human pyruvate dehydrogenase complex. PhD thesis, University of Glasgow, Glasgow

34 Hodgson, J. A., De Marcucci, O. G. and Lindsay, J. G. (1986) Lipoic acid is the site of substrate-dependent acetylation of component X in ox heart pyruvate dehydrogenase multienzyme complex. Eur J Biochem. **158**, 595-600

35 McCartney, R. G., Sanderson, S. J. and Lindsay, J. G. (1997) Refolding and reconstitution studies on the tranacetylase-protein X (E2/X) subcomplex of the mammalian pyruvate dehydrogenase complex: evidence for specific binding of the dihydrolipoamide dehydrogenase component to sites on reassembled E2. Biochemistry **36**, 6819-6826.

36 Singh, G., Brown, A. E., Richman, S. D., Cao, Z., Al-Amodi, H., Kelly, S. M., McGow, D. P., Byron, O., Brown, G. K. and Lindsay, J. G. (2011) Analysing human gene defects with a recombinant model of the human pyruvate dehydrogenase complex. Proc Natl Acad Sci, U S A. (submitted)

37 Zhou, Z. H., Liao, W., Cheng, R. H., Lawson, J. E., McCarthy, D. B., Reed, L. J. and Stoops, J. K. (2001) Direct evidence for the size and conformational variability of the pyruvate dehydrogenase complex revealed by three-dimensional electron microscopy. The "breathing" core and its functional relationship to protein dynamics. J Biol Chem. **276**, 21704-21713

38 Stoops, J. K., Baker, T. S., Schroeter, J. P., Kolodziej, S. J., Niu, X. D. and Reed, L. J. (1992) Three-dimensional structure of the truncated core of the *Saccharomyces cerevisiae* pyruvate dehydrogenase complex determined from negative stain and cryoelectron microscopy images. J Biol Chem. **267**, 24769-24775

39 Wagenknecht, T., Grassucci, R., Radke, G. A. and Roche, T. E. (1991) Cryoelectron microscopy of mammalian pyruvate dehydrogenase complex. J Biol Chem. **266**, 24650-24656

TABLES

Subunit stoichiometry rhE2/E3BP:dE3	Radius of gyration R_g (Å)	Intensity *I(0)*
12+0	143 ± 2	4.3347 ± 1
12+2	145 ± 1	6.3374 ± 1
12+4	151 ± 1	8.0913 ± 1
12+6	157 ± 1	10.922 ± 1
12+8	160 ± 1	13.431 ± 1
12+10	162 ± 1	14.838 ± 1
12+12	162 ± 1	15.183 ± 1
12+14	162 ± 1	15.108 ± 1
12+16	162 ± 1	15.038 ± 1
12+18	162 ± 1	14.965 ± 1

Table 1 R_g determined by SANS from rhE2/E3BP:dE3 samples.

I(0) represents intensity at zero scattering angle.

Model	Stoichiometry	Ratio of E2:E3BP Lipoyl domains	Theoretical radio-labeled E2:E3BP ratio
Addition	60E2+12E3BP	120:12	10:1
Substitution	48E2+12E3BP	96:12	8:1
Variable substitution	46E2+14E3BP	92:14	6.5:1
	44E2+16E3BP	88:16	5.5:1
	42E2+18E3BP	84:18	4.6:1
	40E2+20E3BP	80:20	4:1

Table 2 Core stoichiometries and their theoretical [^{14}C] radio-labeled E2:E3BP ratios

Samples	[^{14}C] counts E2	[^{14}C] counts E3BP	Ratio E2:E3BP
bE2/E3BP$_1$	6025 ± 489	752 ± 31	8.03 ± 0.53:1
bE2/E3BP$_2$	5640 ± 480	718 ± 66	7.92 ± 0.97:1
bE2/E3BP$_3$	2038 ± 95	250 ± 20	8.20 ± 0.57:1
bE2/E3BP$_4$	3230 ± 125	398 ± 40	8.19 ± 0.76:1
rhE2/E3BP$_1$	7802 ± 568	1908 ± 230	4.15 ± 0.33:1
rhE2/E3BP$_2$	19325 ± 1309	4558 ± 93	4.24 ± 0.09:1
rhE2/E3BP$_3$	17967 ± 267	4364 ± 11	4.12 ± 0.01:1
rhE2/E3BP$_4$	4688 ± 110	832 ± 10	5.63 ± 0.02:1

Table 3 Determination of subunit composition of bovine and recombinant E2/E3BP cores via [^{14}C]-NEM radio-labeling.

Subscripts 1 to 4 denote different protein preparations used for the experiment. Average counts of triplicate samples ± SEM (standard error of the mean) are shown.

Core organisation	No. of homotrimers	No. of heterotrimers	No. of final states/solutions
60E2+0E3BP	20	0	1
58E2+2E3BP	18	2	1
56E2+4E3BP	16	4	2
54E2+6E3BP	14	6	3
52E2+8E3BP	12	8	4
50E2+10E3BP	10	10	6
48E2+12E3BP	8	12	7
46E2+14E3BP	6	14	5
44E2+16E3BP	4	16	4
42E2+18E3BP	2	18	3
40E2+20E3BP	0	20	2

Table 4 Plausible E2/E3BP core organisations, corresponding numbers of homo- and hetero-trimers and the number of final states/solution.

FIGURE LEGENDS

Figure 1 Binding stoichiometry of rhE3 to the rhE2/E3BP core assembly determined by GFC and AUC

(A) rhE2/E3BP:rhE3 samples, prepared by maintaining rhE2/E3BP at 421 nM and varying rhE3 levels to satisfy ratios ranging from 3:1 (48E2/12E3BP:4E3) to 1:3 (48E2/12E3BP:36E3), were analysed on a Sephacryl S-300 column (120 ml bed volume) with uncomplexed rhE2/E3BP and rhE3 as controls. Free rhE3 is observed from a ratio of 1:1 onwards, consistent with 2:1 E3BP:E3 binding. **(B)** For AUC sedimentation velocity analysis, samples were maintained at 191.5 nM and the rhE3 concentration varied to achieve ratios from 4:1 (48E2/12E3BP:3E3) to 1:4 (48E2/12E3BP:48E3). *c(s)* analysis of the data again indicates a 2:1 (E3BP:E3) relationship as the low s peak corresponding to free E3 is apparent only at rhE2/E3BP:rhE3 ratios of 1:1 and below.

Figure 2 Binding stoichiometry of dE3 to rhE2/E3BP measured by SANS

(A) SANS curves were acquired for protonated rhE2/E3BP complexed with dE3 at ratios ranging from 0-18 E3 dimers per core. The rhE2/E3BP:dE3 complex was formed initially by maintaining rhE2/E3BP at 1.04 μM prior to dE3 addition at the required molarity to give an E2/E3BP+E3 subunit composition of 48/12+2. Thereafter, equivalent amounts of dE3 were added stepwise, covering the stoichiometry range from 48/12+2 to 48/12+18. Free rhE2/E3BP and dE3 were used as controls. **(B)** *I(0)* normalized for concentration and plotted against the number of dE3 per core indicates saturation at a ratio of 10:1 (dE3:rhE2/E3BP).

Figure 3 Stoichiometry of binding of rhE3 to rhE2/E3BP and bE2/E3BP core assemblies determined by ITC

ITC measurements of rhE3 binding to **(A)** rhE2/E3BP and **(B)** bE2/E3BP cores are shown. Typically, a 1 μl pre-injection was followed by 28 injections (10 μl, at 3 min intervals) of 210 μM or 23 μM rhE3 into the reaction cell containing 1.4 ml rhE2/E3BP (1.09 μM) or bE2/E3BP (0.34 μM), respectively. Corrections for heats of ligand and protein dilution were obtained by injecting rhE3 into buffer and buffer into protein, respectively. The top panel represents changes in binding enthalpy that arise from titrating E3 into E2/E3BP. The bottom panel shows the binding isotherm obtained by integrating the heat of binding at every injection, to which the best fit is obtained using ORIGIN v7.0. Distinct molar ratios of 9.68 and 5.70 were obtained for rhE3 bound to recombinant rhE2/E3BP and bovine bE2/E3BP cores, respectively.

Figure 4 Glutaraldehyde cross-linking of E3BP

SDS-PAGE of full-length rhE3BP before (-) or after (+) chemically cross-linking with 2% (v/v) glutaraldehyde indicates weak covalent dimerisation. Homodimeric rhE3 was used as a control. Molecular masses of markers (lane M) are shown in kDa. Monomeric rhE3BP runs at a lower apparent subunit molecular mass after glutaraldehyde treatment because intra-molecular cross-links produce a more compact species with a higher mobility in the gel.

Figure 5 Mathematical modelling of E2/E3BP core organization

(A) Mathematical modeling of the final states for the different core models follows a near Gaussian distribution, peaking at the 48E2+12E3BP core composition. Various arrangements of E2 (black) and E3BP (orange) on the core faces are shown. In square brackets above each diagram ([X,Y,Z]) are the numbers of core faces that incorporate 3, 4, or 5 pairs of E2s, respectively, for core models of **(B)** 40E2+20E3BP and **(C)** 48E2+12E3BP. The schematic is drawn as a 2D diagram looking along the 5-fold axis of symmetry; the outermost face is denoted by an arrow.

Figure 6 Cross-bridge formation in human PDC

Cylindrical domain model of hPDC, in which E1 heterotetramers (orange) form cross-bridges between E2 monomers (blue), and E3 dimers (green) form cross-bridges between E3BP monomers (grey). The lipoyl domains (LD) and subunit binding domains (SBD) of E2 (dark- and mid-blue respectively) and E3BP (dark- and mid-grey respectively) are connected by linkers (light blue and grey). The specific model illustrated corresponds to the [0,12,0] 48E2+12E3BP arrangement shown in Fig. 4C. Views are along the **(A)** 2-fold **(B)** 3-fold and **(C)** 5-fold axes of symmetry. The figure was drawn using the Google SketchUp Tool (http://sketchup.google.com/).

Figure 1

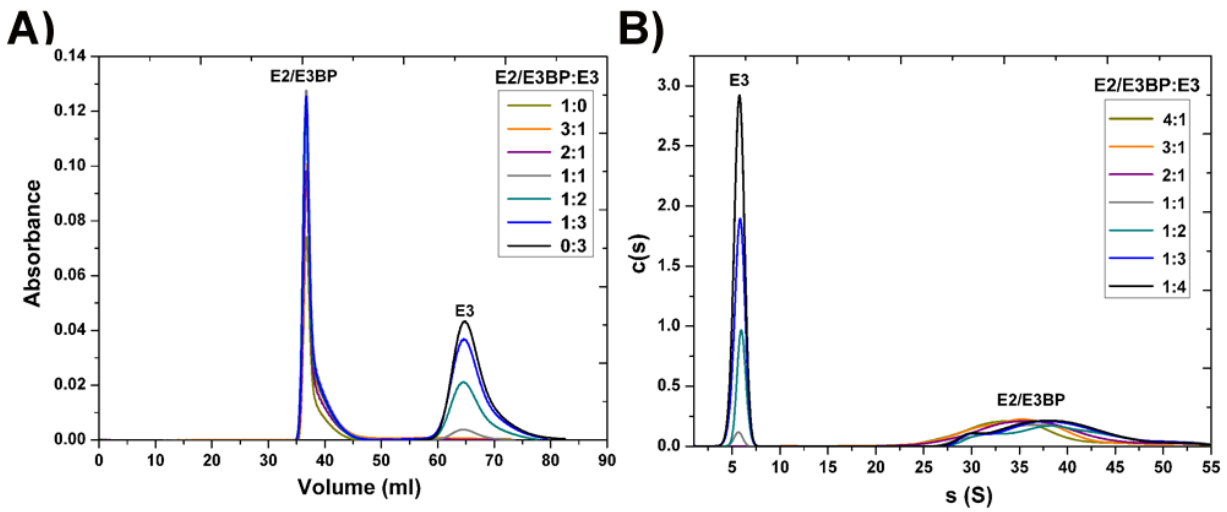

Figure 2

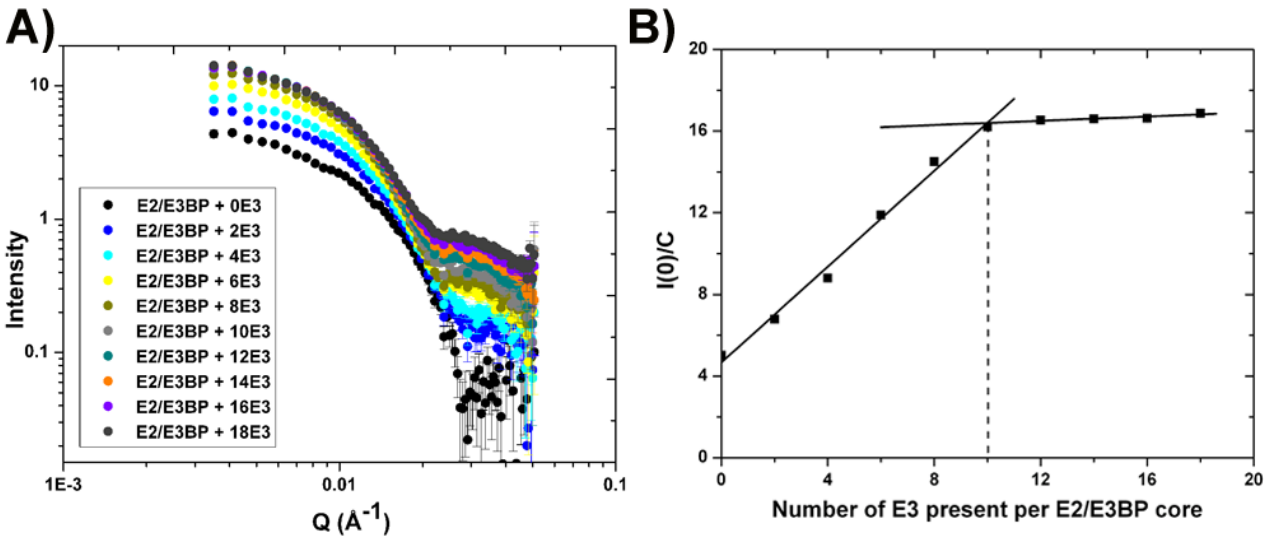

Figure 3

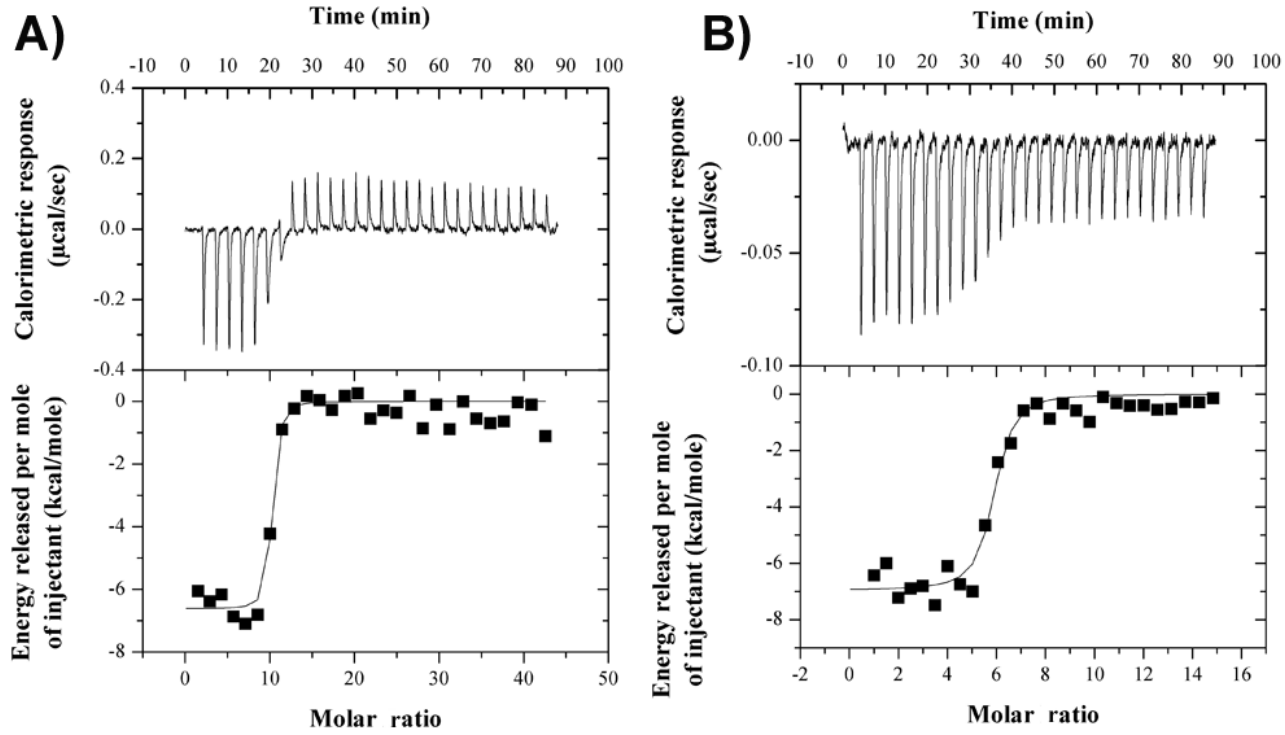

Figure 4

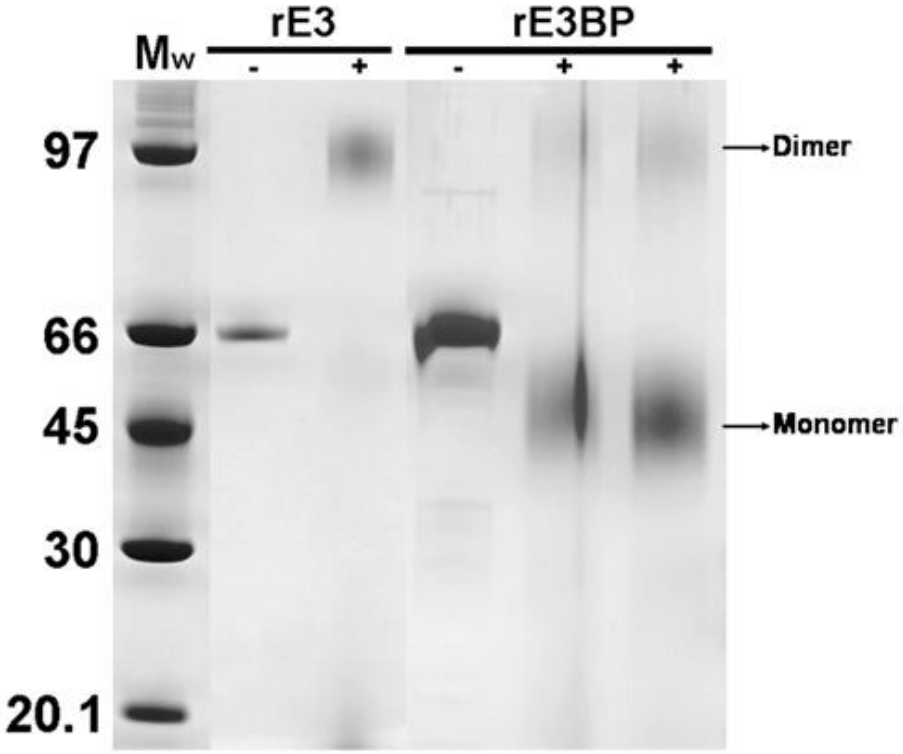

Figure 5

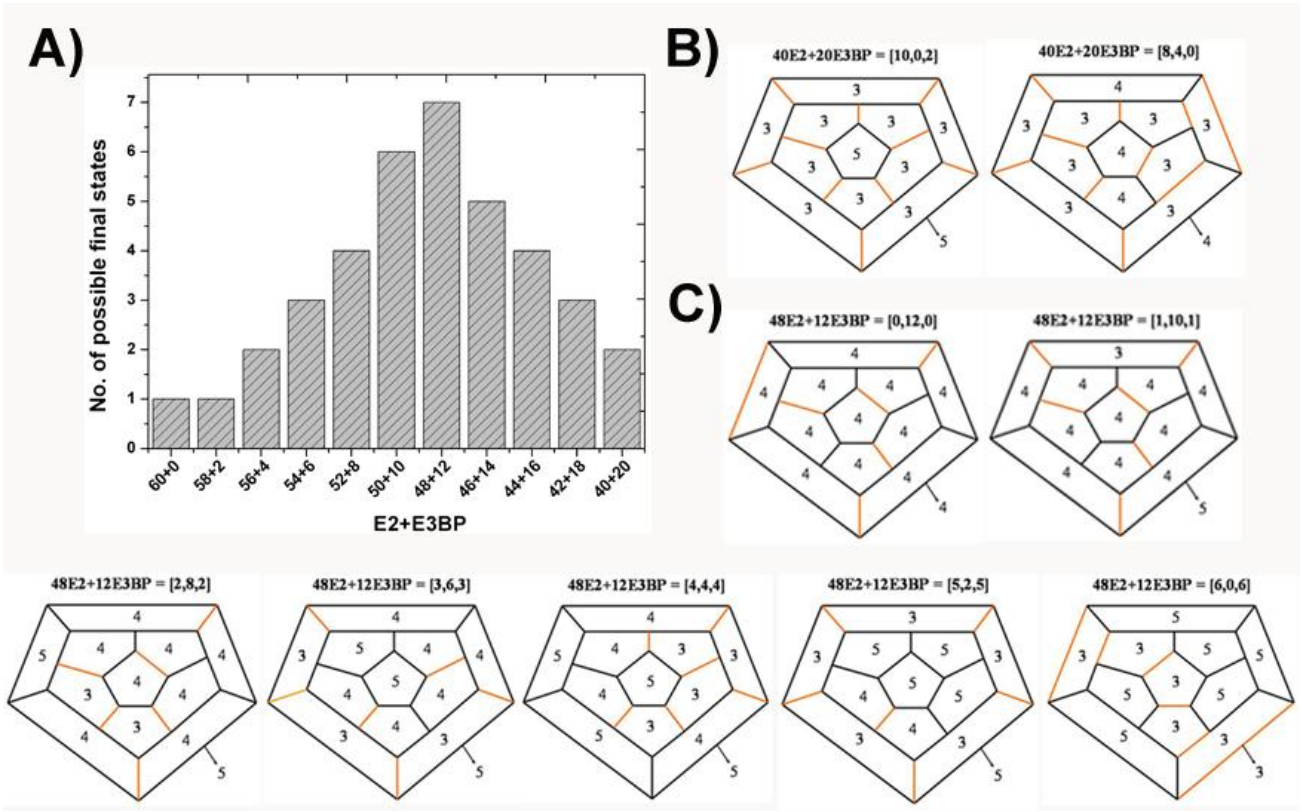

Figure 6

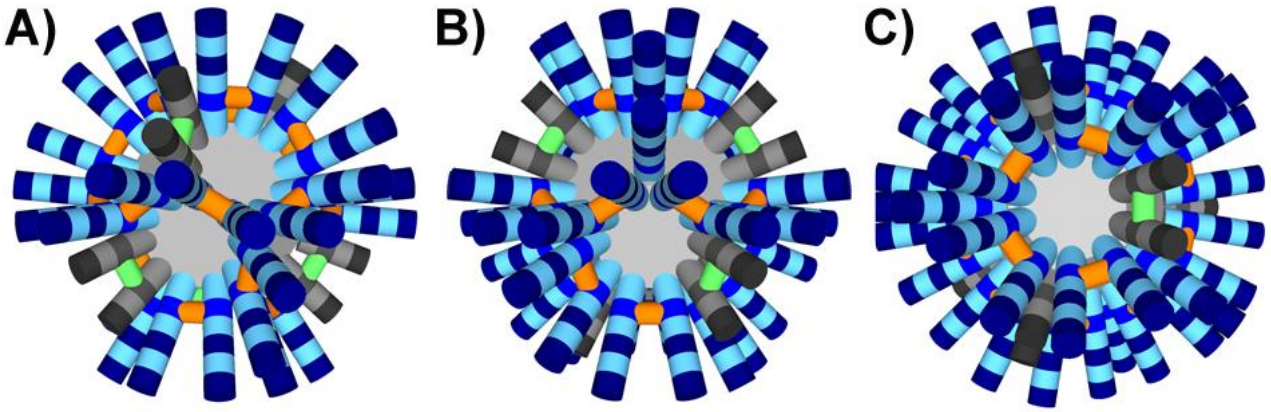

Supplementary Information

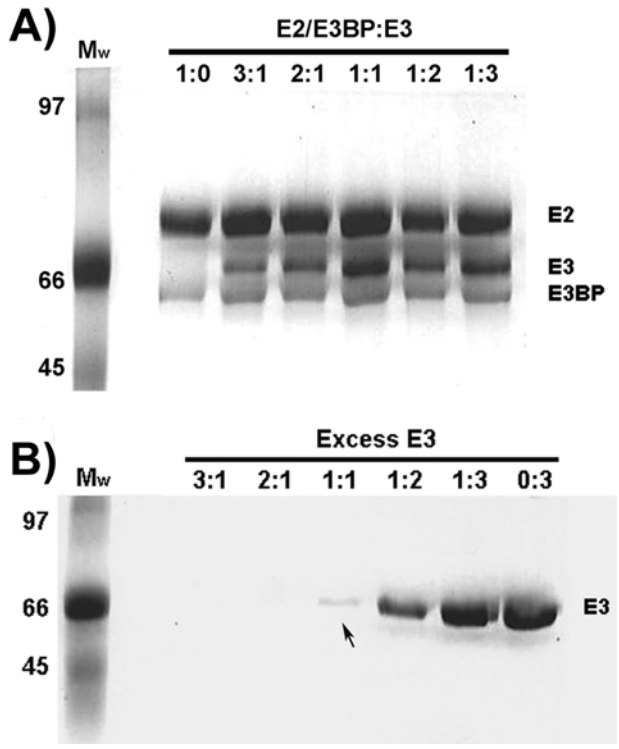

Figure S1 SDS-PAGE analysis of rhE2/E3BP:rhE3 stoichiometry
Peak fractions from GFC separation of rhE2/E3BP:rhE3 at a range of stiochiometries were analysed by SDS-PAGE. **(A)** Void volume (38 ml) GFC peak fractions confirm the incorporation of rhE3 in the complex. **(B)** GFC peak fractions collected at an elution volume of 65 ml show the appearance of excess rhE3 from a 1:1 ratio onwards (arrow). Molecular weights (Mw) are in kDa.

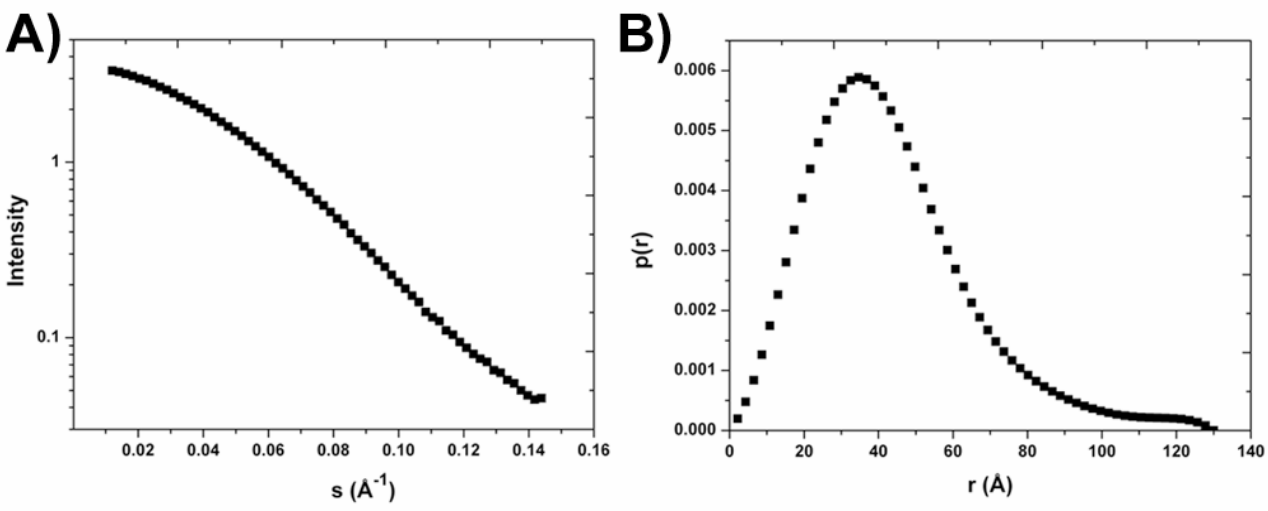

Figure S2 Small angle neutron scattering from deuterated dE3
(A) The SANS curve of uncomplexed dE3. **(B)** The distance distribution function, *p(r)* calculated using GNOM yielded a D_{max} of 130 Å.

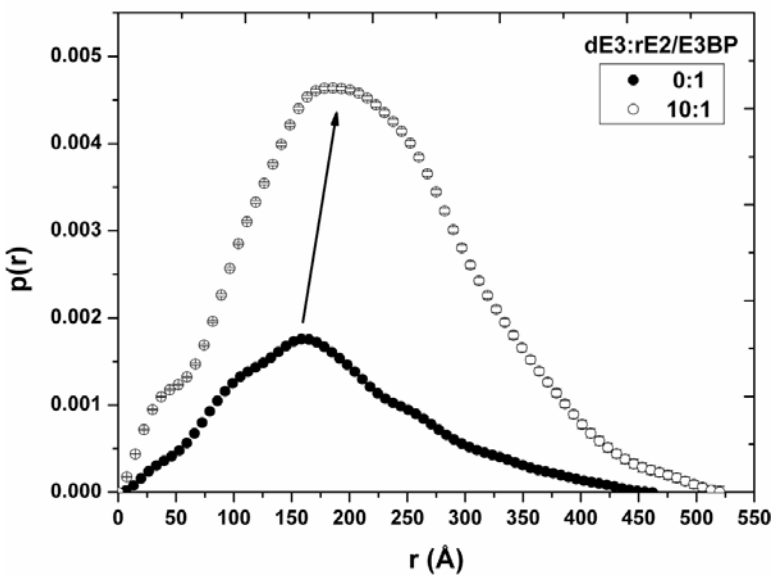

Figure S3 Distance distribution *p(r)* analysis of dE3:rhE2/E3BP at 10:1 saturation
The *p(r)* distributions were calculated using GNOM for uncomplexed rhE2/E3BP and dE3:rhE2/E3BP complex at a binding saturation ratio of 10:1. The radial shift to higher *r* upon dE3 binding to the core is denoted by an arrow. Error bars are shown but are not clearly visible due to their small size.

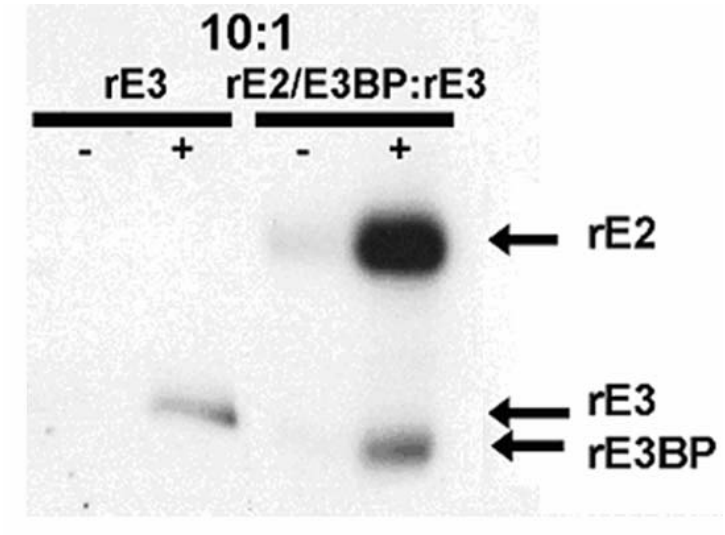

Figure S4 [^{14}C]-NEM fluorography of recombinant PDC core
Specific [^{14}C]-NEM incorporation into E2 and E3BP subunits of rhE2/E3BP core complexed with rhE3 at a molar ratio of 10:1 in the presence of NAD (-) and NADH (+) is denoted. An equivalent amount of uncomplexed rhE3 radiolabelled in the presence of NAD^+ (-) or NADH (+) was included as a control.

Tables

E3BP:E3 stoichiometry		
2:1	**1:1**	
Number of E3 dimers per rhE2/E3BP core		**Core composition**
10*	20	40E2+20E3BP
6	12	48E2+12E3BP

Table S1 Variable substitution rhE2/E3BP core models

* The number of dE3 required for saturation, as determined in the SANS stoichiometry study.

Core organisation	No. of homotrimers	No. of heterotrimers
58E2+2E3BP	18	2
56E2+4E3BP	16	4
54E2+6E3BP	14	6
52E2+8E3BP	12	8
50E2+10E3BP	10	10
48E2+12E3BP	8	12
46E2+14E3BP	6	14
44E2+16E3BP	4	16
42E2+18E3BP	2	18
40E2+20E3BP	0	20

Table S2 Plausible E2/E3BP core organizations and corresponding numbers of homo and hetero-trimers